https://doi.org/10.5194/essd-2026-183
Preprint. Discussion started: 23 April 2026

Open Access Earth System Science Data Discussions

Weather station data from the Mount Everest region, Nepal: 3,810-8,810 m above sea level

Arbindra Khadka[1,2], L. Baker Perry[3,4], Tom Matthews[5], Tenzing Gyalzen Sherpa[6], Chitra Bahadur Shrestha[1], Dibas Shrestha[1], Deepak Aryal[1], Subash Tuladhar[7], Niraj Pradhananga[7], Dinkar Kayastha[7], Brian Raichle[4], Peter Athans[8], Dawa Yangzum Sherpa[8], Keith Garrett[9], Garrett Wheeler[10], Tom Young[11], Aurora Elmore[12]

1 Central Department of Hydrology and Meteorology, Tribhuvan University, Kirtipur, Nepal
2 Université Grenoble Alpes, CNRS, IRD, IGE, Grenoble, France
3 Department of Geography (Climatology), University of Nevada, Reno, Nevada, USA
4 Research Institute for Environment, Energy, and Economics, Department of Sustainable Technology & the Built Environment, Appalachian State University, Boone, North Carolina
5 Department of Geography, King's College London, London, UK
6 Khumbu Climbing Centre, Phortse, Nepal
7 Department of Hydrology and Meteorology, Nepal
8 The North Face, Alameda, California
9 Mount Washington Observatory, North Conway, New Hampshire, USA
10 Campbell Scientific, Logan, Utah, USA
11 RM Young, Traverse City, Michigan, USA
12 National Oceanic and Atmospheric Administration, Maryland, USA

Corresponding Author: Arbindra Khadka arbindra.khadka@cdhm.tu.edu.np

https://doi.org/10.5194/essd-2026-183
Preprint. Discussion started: 23 April 2026

Open Access Earth System Science Data Discussions

Abstract

The National Geographic Rolex Perpetual Planet Everest expeditions 2019-2022 installed a network of Automatic Weather Stations (AWSs) to improve understanding of the climate at high altitudes in the Nepal Himalaya. This knowledge is critical in the Mount Everest (Khumbu) region, due to its extreme altitude, popularity amongst trekkers and mountaineers, and its importance as a source of freshwater for downstream communities. Here we present quality controlled (QC) meteorological data from six AWSs from Phortse (3,810 m above sea level, m asl) to Bishop Rock (8,810 m asl) in the Everest region, including the seasonal climatology, and a comparison with ERA5 reanalysis data from the South Col AWS. The data is accessible from https://doi.org/10.5281/zenodo.18849098 (Khadka, 2026).

1. Introduction

Field research in High Mountain Asia (HMA) which has the most glacier area outside of the polar regions (Brun et al., 2017; Pfeffer et al., 2014) is extremely difficult. The region's high altitude results in low barometric pressure (and hence relatively low oxygen availability: Matthews et al., 2020a), and extreme weather, challenging personnel and equipment alike in the task of assembling high-quality, long-term observational datasets (Salerno et al., 2015; Shea et al., 2015; Khadka et al., 2022; Matthews et al., 2020a). However, there are strong incentives to overcome these difficulties. First, the region is an important freshwater source for a vast number of communities downstream (Immerzeel et al., 2010). Second, the extreme weather, combined with steep terrain, places the region at a relatively high risk of hydrometeorological hazards (Miner et al., 2020). Establishing meteorological observational networks both helps to improve understanding of water resource availability in a changing climate, and to reduce hydrometeorological risks.

Within HMA, the Khumbu region has attracted significant research interest (Salerno et al., 2015; Perry et al., 2020; Wagnon et al., 2021; King et al., 2020; Thakuri et al., 2014, 2019; Sherpa et al., 2023; Potocki et al., 2022). Its extreme elevation, comprising the highest (Mount Everest) and fourth-highest (Lhotse) mountains on earth, as well as the highest-elevation glacier combined with its thriving tourism and mountaineering industry, enable altitudinal gradients in meteorological quantities to be assessed across the entire elevational range of HMA glaciers; drive high demand for accurate weather observations and forecasts (due to the high exposure of trekkers and mountaineers); and provide relatively strong logistical support for fieldwork.

Compared to elsewhere in HMA, the Khumbu region has already been relatively well instrumented with Automatic Weather Stations (AWSs). For instance, an AWS was deployed at Pyramid (5,035 m asl) by EvK2CNR in 1994, and their network was later extended up to South Col (in 2008) (Salerno et al., 2015). Since 2010, The Institute for Sustainable Development (IRD France; GLACIOCLIM) and Nepalese partners began long-term measurements at Mera glacier up to 6,352 m asl and up to 5,450 m asl along the Changri Nup glacier nearby Khumbu Glacier (Figure 1; Khadka et al., 2022). On Everest's northern slopes, AWSs were installed at the North Col (7,028 m asl) and Ruopula Pass (6,560 m asl) (Yang et al., 2011) though these ceased operation by 2008 and 2010, respectively. More recently, Chinese scientists reportedly installed eight AWSs up to near the summit but these data remain unpublished (The Himalayan Times, 2022) and the state of the network remains unknown.

Despite significant investments by numerous research groups, critical gaps persist in understanding HMA cryospheric processes, climate change signals, and data dependability. Weather forecasts for peaks above 6,000 m asl—of life-and-death relevance for the region's many mountaineers (Matthews et al., 2020a), also remain highly uncertain due to the lack of ground-validated observations. Furthermore, a scarcity of high-

https://doi.org/10.5194/essd-2026-183
Preprint. Discussion started: 23 April 2026

quality, elevation-dependent datasets hinders efforts to refine regional climate models and downscale reanalysis products, which is necessary to understand longer-term, larger scale climate change in this region (Khadka et al., 2022).

During the 2019–2025 period, our team of researchers installed and maintained AWSs in six different locations along Everest's southern slopes as part of the National Geographic and Rolex Perpetual Planet Everest Expeditions. These stations have since generated novel insights, including: seasonal oxygen availability at high elevations and climate-influenced changes in Everest's physiological summit height (Matthews et al., 2020b); sublimation dynamics at South Col Glacier (Sherpa et al., 2023); seasonal variability in cloud cover and visibility (Grey et al., 2022); extreme solar irradiance patterns (Matthews et al., 2020a); energy balance studies (Matthews et al., 2020a; Potocki et al., 2022; Brun et al., 2023); and monsoon behaviour at extreme altitudes (Perry et al., 2020; Khadka et al., 2021).

In this paper, we focus on describing the latest available open-access data (https://doi.org/10.5281/zenodo.18849098; Khadka, 2026). We first provide a summary of the network (Section 2), before outlining quality control (QC, Section 3). We close (Section 4) by summarizing the seasonal climatology at stations with the most complete records, the correspondence between AWS observations and ERA5 at the South Col, and by sharing new insights from the highest stations with more intermittent records.

2. Observation area and Data

The geographical locations of the different AWSs are shown in Figure 1. The five stations were initially installed in the primary Khumbu valley from Phortse (3,810 m asl; hereafter referred as PH), Base Camp (5,315 m asl; hereafter referred as BC) Camp II (6,464 m asl; hereafter referred as CII) South Col (7,945 m asl; hereafter referred as SC) and Balcony (8,430 m asl; hereafter referred as BA) during the 2019 expedition (Matthews et al., 2020a). The BA station was toppled by extreme winds and anchor failure in January 2020, so in May 2022 a team of researchers and Sherpa returned to install a new AWS at Bishop Rock (8,810 m asl; hereafter referred as BR), remove the BA station, and upgrade the station at the SC (Matthews et al., 2022).

Data have been recorded using Campbell scientific CR1000X dataloggers, at intervals ranging from 10 minutes to daily. However, here we present quality-controlled hourly data sets in University Coordinated Time (UTC). The respective variables and sensors include air temperature (T), relative humidity (RH), wind speed (WS), radiation variables (Incoming (in) and outgoing (out) shortwave (SW) and long wave (LW) radiation), pressure (Pa), and precipitation (P) (Table 1). We also include data from experimental pitot wind sensors installed at the SC and BR in 2022.

https://doi.org/10.5194/essd-2026-183
Preprint. Discussion started: 23 April 2026

Open Access Earth System Science Data Discussions

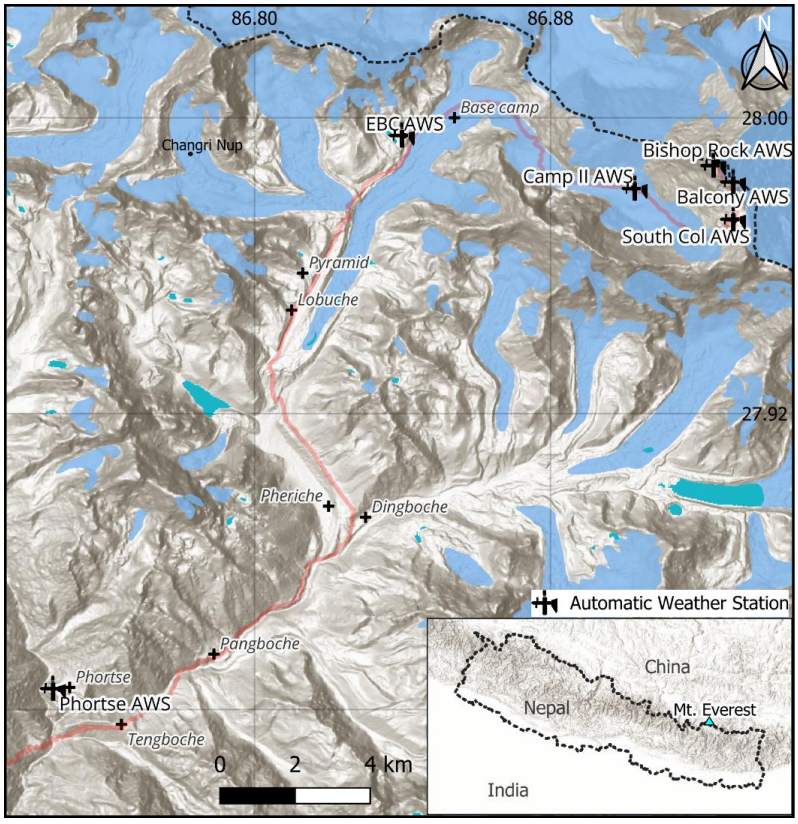

Figure 1. Geographical location of different automatic weather stations in the Khumbu region of Nepal. The plus symbol represents camps in the valley including Everest Base Camp and the Changri Nup point is the area where Meteorological glaciological observation has been monitored since 2010 and the red lines represents the normal climbing route to Mount Everest from South side.

2.1 AWS details and measured variables

Two types of tripods were used for the AWSs: the Campbell Scientific CM106B, which has an adjustable height of between 2.1 and 3 m, was used for the lower three (PH, BC and CII) AWSs. The tripod was affixed with a datalogger box, solar panel, various sensors and an antenna for grounding to protect against lightning (Table 1, see Supplementary Information for photographs). An OTT HydroMet Pluvio^2 with a double alter shield was installed separately at the PH and BC AWSs to measure precipitation. For the upper three (SC, BA and BR) AWSs, a 7-kg custom aluminium tripod designed by Campbell Scientific specifically for Everest was used (Matthews et al., 2020a). The PH and BC AWSs were secured in the soil with stakes pushed 0.5–1 m into the ground, while the other higher AWSs were bolted on to rocks and also guyed to additional anchor points. For the lower AWSs, the batteries were installed inside the data logger box and on a tripod. For the upper AWSs, the batteries were installed in a separate insulated box to protect it from very low temperatures, and both data logger and battery boxes were separately bolted to the rock to reduce wind drag on the tripod. The overall weight of the lower AWSs is approximately 60 kg and the upper AWSs weigh 52 kg, including the additional pitot tube (~2 kg) and other sensors added in 2022 (Matthews et al., 2020a, 2022). The BA AWS was found to have been toppled during the 2020 maintenance visit, possibly due to extreme wind gusts; however, the other tripods remain in position at the time of writing. Below, we

https://doi.org/10.5194/essd-2026-183
Preprint. Discussion started: 23 April 2026

detail measurement details for the respective meteorological variables. This information is also summarised in Table 1.

2.1.1 Air Temperature and Relative Humidity

Air temperature (°C) and relative humidity (%) are measured using a Vaisala HMP155A-L5-PT sensor installed in a naturally ventilated METSPEC 14-plate solar radiation shield. Additionally, a CS109 temperature probe, ventilated by a METSPEC 6-plate solar radiation shield, was installed for air temperature measurement at each station in 2019. While both shield types reduce radiative heating, the absence of active aspiration, particularly for the less protected CS109 with its 6-plate shield may introduce a positive diurnal temperature bias. In 2022, however, only dual Vaisala HMP 155A-L5-PT sensors with METSPEC 14-plate solar radiation shields were installed in the SC and BR AWSs. The sensors are installed 2 m from the ground for the PH, BC and CII AWSs, and 1.5 m for the higher AWSs.

2.1.2 Wind Speed and Direction

Initially, in 2019, the R.M. Young 05108-45 was used in all AWSs for measuring wind speed and direction. The SC and BA had two of these sensors for redundancy. However, all four R.M. Young 05108-45s failed in the extreme conditions encountered at the BA and SC. We therefore replaced the double 05108-45s at the SC with a new polycarbonate version of that sensor; we also added a Richards C5C anemometer and Pitot tube, custom made by the Mount Washington Observatory. This same sensor array for measuring wind speed was used at the BR station after the demise of the BA AWS (Matthews et al., 2022). All wind sensors were installed 2.3 m above the ground surface for lower AWSs (PH-CII) and ~2 m for higher AWSs (SC, BA, and BR).

2.1.3 Air Pressure

The measurement of barometric air pressure (hPa) at PH is achieved using the Vaisala PTB 110, whilst the Vaisala PTB210 is employed in all other AWSs as higher AWSs weather is comparatively harsh with lower pressure. The sensors are installed within the data logger box of all AWSs. However, the data logger box of the three lower AWSs (PH, BR, and CII) is located on the tripod mast, at a distance of 1-1.5 m above the ground surface.

2.1.4 Radiation

The measurement of the four components of radiation is facilitated by the Hukseflux SR30 (up/down shortwave radiation); Hukseflux IR20 (up/down longwave radiation) at PH; Apogee SN-500-SS at CII; and Hukseflux NR01 at other AWSs using the cross arm (Figure S1, S2). The radiation sensors are mounted on crossarms at approximately 1.5 m above the surface at all locations.

2.1.5 Precipitation

At the PH and BC AWSs, the weighing OTT Pluvio^2 was installed with double alter shields, with a height of 1.5 m (from the surface at the mouth of Pluvio). At both sites the OTT Pluvio^2 is partially filled with an ecologically friendly antifreeze agent, which is replaced regularly when the reservoir is emptied during regular maintenance visits.

2.1.6 Time Lapse Photo

In addition to the the meteorological measurement at BC AWS, a Campbell Scientific CCFC Field Camera was installed looking eastward toward the summit of Mt Everest. The camera captures photographs two times a day; at 0937 Nepal time (NPT) (0352 UTC) and at 1437 NPT (0852 UTC), respectively (Grey et al., 2022).

2.2 Real-time data transfer

At the beginning (2019) all the stations (except PH) were configured to transmit real-time data using the Thuraya satellite network. After the failure of the Thuraya 3 satellite in April 2024, connectivity became

https://doi.org/10.5194/essd-2026-183
Preprint. Discussion started: 23 April 2026

intermittent, and then stopped altogether. In 2025, we therefore moved BC and CII to the Iridium Short Burst Data (SBD), as used by other remote networks (e.g., on the Greenland Ice Sheet: Fausto et al., 2021). The SC station was not converted to Iridium SBD in 2024 due to logistical, financial, and time constraints and therefore limited data are only currently available via data via direct download. The PH station was originally configured to transfer data using the network but was switched to the Nepal Telecom 4G network in 2024. Though only limited variables are transmitted through SDB, the new data transmitted from SDB and BGAN-INMARSAT are not included in the https://doi.org/10.5281/zenodo.18849098 (Khadka, 2026). The new data will be added after the next fieldwork probably in spring 2026.

https://doi.org/10.5194/essd-2026-183
Preprint. Discussion started: 23 April 2026

Open Access Earth System Science Data Discussions

170 *Table 1. AWSs location, data availability, sensors and their height from the surface during the installation (updated from*
171 *Mattmendhews et al. 2020a).*

	Phortse (PH)	**Base Camp (BC)**	**Camp II (CIII)**	**South Col (SC) 2019**	**South Col (SC) 2022**	**Balcony (BA)**	**Bishop Rock (BR)**
Lat, Lon, and Elevation	27.8456°N 86.7472°E 3,810 m	27.9952°N 86.8406°E 5,315 m	27.9810°N 86.9023°E 6,464 m	27.9719°N 86.9295°E 7,945 m	27.9719°N 86.9295°E 7,945 m	27.9826°N 86.9292°E 8,430 m	27.98805°N 86.92521°E 8,810 m
Data availability	April 2019 to present	October 2019 to-present	May 2019 to present	June 2019 to July 2021	May 2022 to present	May 2019 to January 2020	May 2022 to July 2023
Sensor level above ground (m)	2 m for temperature and humidity, 2.3 m for wind	2 m	2 m	1.5 m for temperature and humidity, 2m for wind	1.5 m for temperature and humidity, 2m for wind	1.5 m for temperature and humidity, 2 m for wind	1.5 m for temperature and humidity, 2 m for wind
Air temperature sensor **Relative humidity sensor**	Vaisala HMP155A-L5-PT; CS109 Vaisala HMP155A-L5-PT	Vaisala HMP155A-L5-PT; CS109 Vaisala HMP155A-L5-PT	Vaisala HMP155A-L5-PT; CS109 Vaisala HMP155A-L5-PT	Vaisala HMP155A-L5-PT; CS109 Vaisala HMP155A-L5-PT	2 × Vaisala HMP155A-L5-PT 2 × Vaisala HMP155A-L5-PT	Vaisala HMP155A-L5-PT; CS109 Vaisala HMP155A-L5-PT	2 × Vaisala HMP155A-L5 2 × Vaisala HMP155A-L5-PT
Wind speed and direction sensor	R.M. Young 05108-45	R.M. Young 05108-45	R.M. Young 05108-45	2 × R.M. Young 05108-45	Polycarbonate R.M. Young 05108-45, Richards C5C anemometer, Pitot tube	2 × R.M. Young 05108-45	Polycarbonate R.M. Young 05108-45 05108, Richards C5C anemometer, Pitot tube
Air Pressure sensor	Vaisala PTB 110	Vaisala PTB210	Vaisala PTB210	Vaisala PTB210	Vaisala PTB210	Vaisala PTB210	Vaisala PTB210
Radiation sensor	2 × Hukseflux SR30 (up/down shortwave radiation); 2 × Hukseflux IR20 (up/down thermal radiation)	Hukseflux NR01	Apogee SN-500-SS	Hukseflux NR01	Hukseflux NR01	Hukseflux NR01	Hukseflux NR01
Precipitation sensor	OTT Pluvio^2 and double alter shield	OTT Pluvio^2 and double alter shield	-	-	-	-	-
Time Lapse Photo	-	Campbell Scientific Canada CCFC Field Camera	-	-	-	-	-
Present weather sensor	OTT Parsivel^2	OTT Parsivel^2	-	-		-	-
Relative surface elevation change sensor	Campbell Scientific SR50A	Campbell Scientific SR50A	Campbell Scientific SR50A	-	-	-	-
Data Logger	Campbell Scientific CR1000X	Campbell Scientific CR1000X	Campbell Scientific CR1000X	Campbell Scientific CR1000X	Campbell Scientific CR1000X	Campbell Scientific CR1000X	Campbell Scientific CR1000X
Logger enclosure	Standard Campbell Scientific	Standard Campbell Scientific	Standard Campbell Scientific	Pelican case with military-spec quick-connects	Pelican case with military-spec quick-connects	Pelican case with military-spec quick-connects	Pelican case with military-spec quick-connects
Batteries	24 Ah	3 × 8Ah	3 × 8Ah	3 × 8Ah	3 × 8Ah	3 × 8Ah	3 × 8Ah

https://doi.org/10.5194/essd-2026-183
Preprint. Discussion started: 23 April 2026

Charging	2 × 20W solar panels	2 × 20W solar panels	2 × 20W solar panels	2 × 10W solar panels	3 × 10W solar panels	2 × 10W solar panels	3 × 10W solar panels
Telemetry	Inmarsat, Sierra wireless with NTC sim	Thuraya; 400 MHz radio, Iridium	Thuraya; 400 MHz radio, Iridium	Thuraya; 400 MHz radio	Thuraya; 400 MHz radio	Thuraya; 400 MHz radio	Thuraya; 400 MHz radio
Sampling interval	3 s (wind); 60 s (radiation, air pressure, temperature, relative humidity, precipitation) 3600 s (present weather, relative surface elevation change)	5 s (wind); 60 s (temperature, relative humidity, precipitation); 600 s (air pressure); 3600 s (present weather)	60 s (temperature, relative humidity, wind); 600 s (radiation); 3600 s (relative surface elevation change)	5 s (wind); 60 s (temperature, relative humidity, radiation); 600 s (pressure)	5 s (wind); 60 s (temperature, relative humidity); 600 s (pressure)	5 s (wind); 60 s (temperature, relative humidity); 600 s (pressure)	5 s (wind); 60 s (temperature, relative humidity); 600 s (pressure)
Tripod	Campbell Scientific CM106B	Campbell Scientific CM106B	Campbell Scientific CM106B	Custom Aluminum	Custom Aluminum	Custom Aluminum	Custom Aluminum
Approximate Weight	Not available	Not available	Not available	Total: 50 kg Pelican case with logger: 8 kg Pelican case with batteries: 16 kg Tripod: 7 kg Crossarms, mounts, and bolts: 11 kg Sensors: 8 kg	Total: 52 kg Pelican case with logger: 8 kg Pelican case with batteries: 16 kg Tripod: 7 kg Crossarms, mounts, and bolts: 11 kg Sensors: 10 kg	Total: 50 kg Pelican case with logger: 8 kg Pelican case with batteries: 16 kg Tripod: 7 kg Crossarms, mounts, and bolts: 11 kg Sensors: 8 kg	Total: 52 kg Pelican case with logger: 8 kg Pelican case with batteries: 16 kg Tripod: 7 kg Crossarms, mounts, and bolts: 11 kg Sensors:10 kg

3. Data treatment and quality control procedure

Data gaps, sensor failures, and erroneous readings were common due to factors such as riming (icing of sensors), heavy snowfall partially or completely burying the upper stations, battery depletion, extreme temperature fluctuations, and communication failures. Acknowledging these challenges, we implemented, a multi-stage quality control (QC) procedure to identify and flag spurious data points.

Our QC protocol takes a tiered approach, progressing from simple flagging to more complex, variable-specific corrections. The procedures applied to the raw dataset are as follows:

Data flagging: Where available, manufacturer-provided diagnostic data (Table S 1) and internal sensor flags were used to identify and filter out physically implausible or erroneous observations.

Relative humidity correction: Physically, RH cannot exceed 100% under stable conditions. Any instances in which RH was greater than 100% were assumed to be caused by sensor uncertainty or rapid cooling events, and were capped at 100%. Artificially low RH in our raw measurements were also present due to the logger program calculating RH with respect to water rather than ice when air temperatures were below 0 °C. We therefore corrected these instances by computing vapour pressure (e) from measured RH, and saturation vapour pressure (e_s) with respect to ice using the air temperature (Buck, 1981, 1996). Corrected RH was hence e/e_s).

https://doi.org/10.5194/essd-2026-183
Preprint. Discussion started: 23 April 2026

Open Access Earth System Science Data Discussions

Wind sensor freezing detection: Periods of zero wind speed coupled with zero wind direction variability are a strong indicator of sensor freezing (e.g., encased in rime ice). These data points were identified and removed from the dataset rather than being treated as valid calm conditions.

Shortwave radiation corrections:

Night time values: All incoming shortwave radiation below 7 W m^{-2} (a common threshold for sensor uncertainty during night time) were set to zero (Shea et al., 2015; Khadka et al., 2022).

Albedo-based correction: Fresh snowfall can cause the surface albedo (α = SWout / SWin) to exceed a realistic value for snow (typically $\alpha \leq 0.95$). For periods where calculated albedo exceeded 0.95, it was assumed that SWin was underestimated (e.g., due to sensor riming or a tilted sensor). SWin was recalculated as SWout /0.95 to provide a more realistic estimate 95 (Shea et al., 2015; Khadka et al., 2022)

Precipitation: The Pluvio^2 weighing precipitation gauges were equipped with double alter shields to minimize wind-induced under-catch (Figure S1). Only positive accumulation records were considered. No correction for wind under-catch was applied in this dataset; users are advised to apply such corrections using established methods (e.g., Kochendorfer et al., 2022).

https://doi.org/10.5194/essd-2026-183
Preprint. Discussion started: 23 April 2026

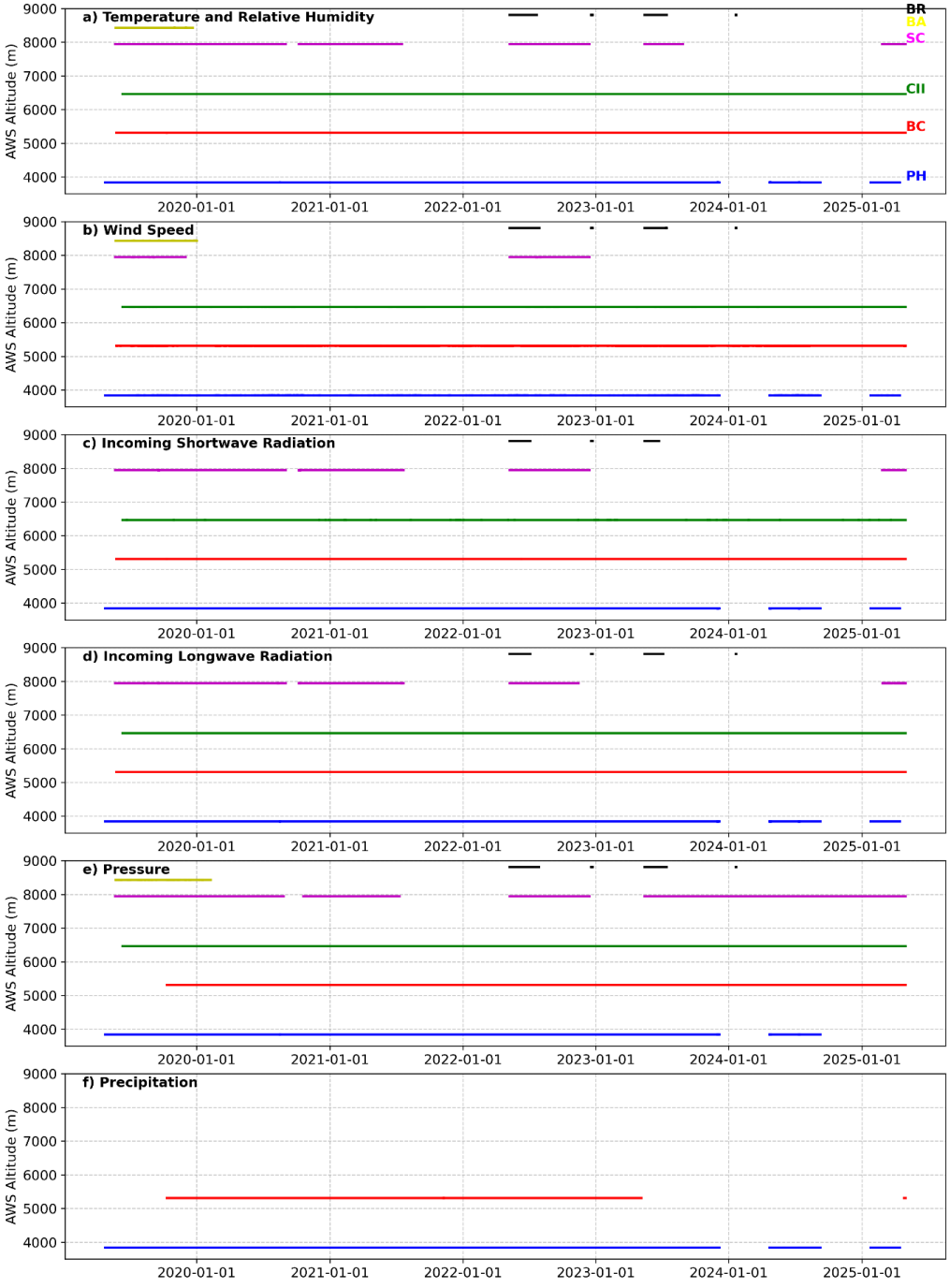

Figure 2. Time periods when stations/sensors were operational since the beginning of installation to the last field visit in May 2025. The solid lines represent the period of available data.

https://doi.org/10.5194/essd-2026-183
Preprint. Discussion started: 23 April 2026

Open Access Earth System Science Data Discussions

4. Climatology of the region

Figure 3 shows the monthly precipitation and temperature (from December 2019 to November 2022; Figure 2) for PH (3,840 m) and BC (5,315 m), the two AWSs in the network that include measurements of precipitation. Whilst this is a very short period for understanding climate variability, there is a clear seasonal pattern in precipitation and temperature at both sites. The annual precipitation is 790 and 629 mm, with 72 and 77% of this falling during the monsoon at the PH and BC AWSs, respectively. The average annual temperature at PH is 4.1 ℃, BC is -3.1 ℃ and CII is -10.2 ℃ with monthly amplitude of temperature is 6.7 (max 8.0 ℃ in March, min 4.6 ℃ in July),6.5 ℃ (max 7.9 ℃ in March, min 4.9 ℃ in December) and 6.4 (max 7.8 ℃ in March, min 3.6 ℃ in December), respectively.

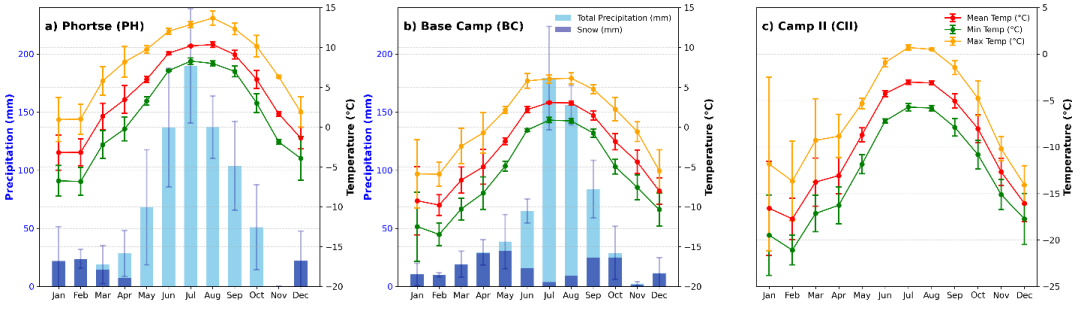

Figure 3. Mean annual cycle of monthly precipitation (snow and total precipitation in mm liquid water equivalent, histograms) and mean monthly mean, minimum and maximum air temperature (T, lines) during December 2019- November 2022 at PH, BC and CII AWSs. The bar represents the standard deviation for all different variables. .

Seasonal mean values, and elevation gradients between the Ph and BC AWSs (separated by ~1500 m) also reveal some interesting characteristics (Table 2). The precipitation gradients average -107 mm km^{-1} (-17 % km^{-1}) average over three years, but it declines by almost 50 % during the monsoon (to -56 mm km^{-1}/12 % km^{-1}). Overall, the amount of precipitation measured at the both (PH and BC) observing sites is higher than the amount measured at the Pheriche (4200 m asl: 540 mm) and Pyramid (5050 m asl: 449 and 591 mm) by IRD stations (Khadka et al., 2022). Similarly, between the PH and BC, the mean temperature gradient is -4.8 ℃ km^{-1} with minimum -4.5 ℃ km^{-1} during the winter and maximum -5.4 ℃ km^{-1} during the Pre-monsoon. Both seasonal and annual temperature gradients (Table 2) are also less negative than reported previously (pre-monsoon, monsoon, annual: -6.5, -5.7, -6.0 ℃ km^{-1}, respectively) by Salerno et al. (2015), calculated using several stations on Koshi basin between ~1,000-8,000 m asl. However, we note that reported non-linearity in the temperature-altitude relationship in the Khumbu region (Khadka et al., 2021) limits the comparability of lapse rates calculated across different elevational ranges.

Table 2. Mean seasonal and annual Temperature (℃) and precipitation (P, mm) at PH and BC AWSs and the calculated Temperature and precipitation gradients (TG and PG) between these AWSs.

	Base Camp (BC)		Phortse (PH)			
Season	Temperature (℃)	Precipitation (mm)	Temperature (℃)	Precipitation (mm)	TG (℃ km^{-1})	PG (mm km^{-1}/% km^{-1})
Winter	-8.8	27	-2.1	56	-4.5	-20/-73
Pre-Monsoon	-4.5	87	3.6	115	-5.4	-19/-22

https://doi.org/10.5194/essd-2026-183
Preprint. Discussion started: 23 April 2026

Monsoon	2.4	484	9.7	567	-4.8	-56/-12
Post-Monsoon	-3.1	31	3.9	51	-4.6	-13/-44
Annual	-3.1	629	4.1	790	-4.8	-107/-17

5. Comparison with ERA5

Monitoring the meteorology at the highest altitudes in the Himalaya at elevations where glaciers are accumulating mass, and where mountaineers are most at risk from extreme weather provides the greatest test to observational efforts. Accordingly there is considerable interest in using reanalysis data to extend brief in-situ records. However, to facilitate such extensions, it is necessary to establish the extent to which such reanalyses products can reproduce the observed meteorology (Khadka et al., 2022). Here, we therefore compare temperature, relative humidity and wind speed between the SC AWS (the longest record from above Camp II, where extreme weather poses the greatest risk for mountaineers) and ERA5 reanalysis (Hersbach et al., 2020) data from the nearest grid point at the 350 hPa pressure level (most representative of the SC: mean air pressure 2019-2021 = 377 hPa).

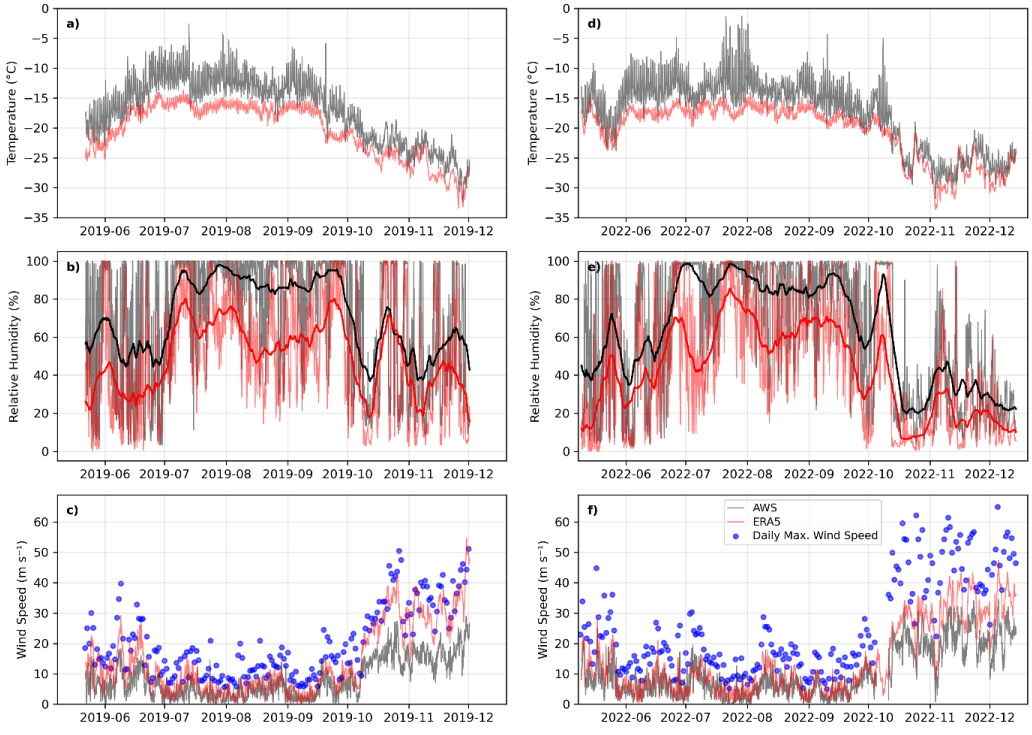

Figure 4. Hourly air temperature, relative humidity (with respect to water) and wind speed from the SC AWS and ERA5 350 hPa pressure level data (from the nearest grid point to the SC AWS) for the available data period of 2019 (a,b,c) and 2022 (d,e,f). The solid dark black and red relative humidity line represesnts the 10 days running mean values.

During both 2019 and 2022, air temperature exhibited reasonably close co-variation between the SC observations and ERA5, with an $R^2 > 0.6$ (Figure 4 and Table 3). ERA5 systematically underestimates air temperature relative to measurement, although some of that reflects the higher altitude (lower air pressure)

https://doi.org/10.5194/essd-2026-183
Preprint. Discussion started: 23 April 2026

at 350 hPa relative to the SC data. Diurnal variability is also considerably greater in the SC dataset (Figure S3 and S4), likely reflecting diurnal fluctuations in the measured surface heat fluxes at SC, which are missing in ERA5 as this (higher altitude) pressure level is representative of the free atmosphere.

The R^2 (0.49 and 0.57) between the AWS and ERA5 relative humidity were adequate for both 2019 and 2022, however the MAE and RMSE for the relative humidity are >20%. From the 10 days running mean both AWS and ERA5 relative humidity clearly shows the seasonal transitions. In 2019 and 2022 the monsoon onset was 1st July and 14th June at SC.

In both years the wind speed exhibited the highest correlation between SC observations and ERA5 (R^2 = 0.70). However, ERA5 consistently overestimates mean winds at the SC (MAE = 4.8 and 5.4 m s^{-1} in 2019 and 2022, respectively (Table 3 and Figure 4). This is again consistent with the ERA5 grid point being representative of the higher-altitude free atmosphere; frictional drag at the SC reduces the wind speed. We also observe faster winds in the post monsoon in 2022 compared to 2019.
Based on the generally good agreement between ERA5 reanalysis data and observations at the SC, we anticipate that the reanalysis could be used to gap-fill and extend intermittent meteorological records from Mt. Everest's upper slopes—correcting the time-varying biases using empirical-statistical, or machine-learning based approaches (Van Wyk de Vries et al., 2024; Potocki et al., 2022).

Table 3. Values of each statistical metrics (R^2, MAE, RMSE) obtained by the comparing the SC AWS measured and ERA5 350 hPa temperature (T), relative humidity (RH) and wind speed (WS) at hourly scale for 2019 and 2022.

Year	Variables	R^2	MAE	RMSE
2019	T (°C)	0.67	3.7	4.1
	RH (%)	0.49	24.6	31.4
	WS (m s^{-1})	0.70	4.8	5.6
2022	T (°C)	0.62	3.1	3.6
	RH (%)	0.57	23.4	30.4
	WS (m s^{-1})	0.70	5.3	6.1

6. Research Insight | Importance of the data

Observations from the SC (Figure 4) highlight the potential for mean winds exceeding 30 ms^{-1} and gusts above 60 ms^{-1} speeds that can be extremely dangerous for mountaineers: at high risk of being blown over, and elevated the probability of cold injury (Sherpa et al., 2023; Van Wyk de Vries et al., 2024). Elsewhere, data from the network of AWSs described here has shown oxygen availability at the summit to be highly variable at synoptic timescales, meaning that the "apparent elevation" of Mt. Everest (how high the mountain would feel for those not breathing supplemental oxygen) can vary by almost 750 m, and that during the most challenging winter conditions an ascent without the aid of supplemental oxygen might be impossible (Matthews et al., 2020b). Accurately forecasting wind speeds and oxygen variability for the upper slopes of Mt. Everest is therefore of high importance for increasing safety on the mountain. The data from the AWSs provided here provide the foundation to achieve such improvements. At the minimum, they can be used to assess uncertainty in the freely-available forecasts widely used by expeditions (Matthews et al., 2020b); but they can also be used to train model output statistics including novel application of machine learning to provide improved, hyper-local forecasts for identifying optimal climbing windows (Van Wyk de Vries et al., 2024).

The AWS data shared here can also be extremely useful for understanding cryosphere-climate interactions at the highest elevations within HMA. For instance, the archive has already been used to estimate the surface energy balances at the summit of Mt. Everest (Matthews et al., 2020a), and for the South Col Glacier (at ~8,000 m asl), revealing a high-altitude system that might be acutely sensitive to changes in effective

https://doi.org/10.5194/essd-2026-183
Preprint. Discussion started: 23 April 2026

precipitation due to extremely high levels of insolation(Matthews et al., 2020a; Potocki et al., 2022; Brun et al., 2023). Yet significant uncertainties remain, not least because the observational record presented here is brief. Understanding here could be improved through extending these observations with downscaled reanalyses products (such as ERA5).

The data here are useful not only for assessing cryosphere-climate interactions at extreme elevations but could be used to improve understanding of surface energy and mass balances within the ablation areas of the region's glaciers, and below. The precipitation measurements, for instance, are particularly high quality--taken behind double Alter shields to reduce under-catch (which likely accounts for the greater accumulations relative to nearby stations without such shields: Pheriche and Pyramid), and hence offer a valuable opportunity to constrain mass inputs. More generally, when used in combination with the generally lower-altitude observations from the GLACIOCLIM and EvK2CNR networks, the data shared here can improve quantification of elevational gradients in key meteorological variables needed in distributed (e.g., glacier or hydrological) modelling assessments across up to approximately five vertical kilometres, and hence the entire glacierised elevational range of the Khumbu region.

Data across such a large elevational range could also provide valuable insight into regional-scale atmospheric dynamics. For instance, the timing and character of the monsoon's arrival—critical in determining the annual precipitation totals (Perry et al., 2020), and a key control on melt energy (Khadka et al., 2021; Matthews et al., 2020a) can be assessed right up to the upper accumulation area of the Khumbu glacier. Important further work might improve understanding of the relevant physical drivers behind elevational differences in the monsoon's arrival, how they interact with local anabatic and potential katabatic forcing, and how they might change with further global warming (Salerno et al., 2023).

Ultimately, though, these data might be used in ways far beyond the illustrations above. The upper slopes of Mt. Everest represented the last frontier for human exploration, reached successfully by humans 42 years after the South Pole was attained. Meteorological measurements from the highest reaches only began in 2022 (at the BR). We are still, therefore, at the very beginnings of exploring the weather of this extreme environment, and the list of questions that these data might help answer from disciplines beyond the climate sciences (e.g., biology: Dragone et al., 2023) might conceivably grow rapidly.

Acknowledgements

This research was conducted in partnership with National Geographic Society (NGS), Rolex, and Tribhuvan University, with approval from all relevant agencies of the Government of Nepal. We acknowledge Sujatha Bagal and all the NGS team for all their support. We also wish to thank the communities of the Khumbu Region, Shangri-La Nepal Treks, Seven Summit Treks, and we further recognize the extraordinary efforts of our entire Sherpa climbing teams since 2019, whose physical and mental prowess at altitude made installation and maintenance of the AWSs possible.

Authors Contribution

BP, TM, and ACE planned the initial data collection strategy. BP and TM managed the funding and collaboration with the National Geographic Society and Rolex for the 2019-2025 period. AK, BP, TM and TGS installed and maintained the AWSs with the Sherpa supports. BP and TM worked closely with Campbell Scientific to design and program the AWSs. AK, BP and TM contributed to the data analysis, manuscript designing. AK prepared the paper with contribution from all the co-authors.

https://doi.org/10.5194/essd-2026-183
Preprint. Discussion started: 23 April 2026

Data availability

The quality controlled data is available at: https://doi.org/10.5281/zenodo.18849098 (Khadka, 2026) moreover the data in csv format and can be downloaded from https://www.nationalgeographic.org/projects/perpetual-planet/everest/weather-data/.

Reference

Brun, F., Berthier, E., Wagnon, P., Kääb, A., and Treichler, D.: A spatially resolved estimate of High Mountain Asia glacier mass balances from 2000 to 2016, Nat. Geosci., 10, 668–673, https://doi.org/10.1038/ngeo2999, 2017.

Brun, F., King, O., Réveillet, M., Amory, C., Planchot, A., Berthier, E., Dehecq, A., Bolch, T., Fourteau, K., Brondex, J., Dumont, M., and Mayer, C.: Everest South Col Glacier did not thin during the period 1984 – 2017, Cryosph., 17, 3251–3268, 2023.

Buck, A. L.: New Equations for Computing Vapor Pressure and Enhancement Factor, J. Appl. Meteorol. Climatol., 20, 1527–1532, https://doi.org/10.1175/1520-0450(1981)020<1527:NEFCVP>2.0.CO;2, 1981.

Buck, A. L.: Buck research cr-1a user's manual, Buck Res. Instruments Boulder, CO, USA, 5, 1996.

Dragone, N. B., Perry, L. B., Solon, A. J., Seimon, A., Seimon, T. A., and Schmidt, S. K.: Genetic analysis of the frozen microbiome at 7900 m a.s.l., on the South Col of Sagarmatha (Mount Everest), Arctic, Antarct. Alp. Res., 55, 2164999, https://doi.org/10.1080/15230430.2023.2164999, 2023.

Fausto, R. S., Van As, D., Mankoff, K. D., Vandecrux, B., Citterio, M., Ahlstrøm, A. P., Andersen, S. B., Colgan, W., Karlsson, N. B., Kjeldsen, K. K., Korsgaard, N. J., Larsen, S. H., Nielsen, S., Pedersen, A., Shields, C. L., Solgaard, A. M., and Box, J. E.: Programme for Monitoring of the Greenland Ice Sheet (PROMICE) automatic weather station data, Earth Syst. Sci. Data, 13, 3819–3845, https://doi.org/10.5194/ESSD-13-3819-2021, 2021.

Grey, L., Johnson, A. V., Matthews, T., Perry, L. B., Elmore, A. C., Khadka, A., Shrestha, D., Tuladhar, S., Baidya, S. K., Aryal, D., and Gajurel, A. P.: Mount Everest's photogenic weather during the post-monsoon, Weather, 77, 156–160, https://doi.org/10.1002/WEA.4184, 2022.

Hersbach, H., Bell, B., Berrisford, P., Hirahara, S., Horányi, A., Muñoz-Sabater, J., Nicolas, J., Peubey, C., Radu, R., Schepers, D., Simmons, A., Soci, C., Abdalla, S., Abellan, X., Balsamo, G., Bechtold, P., Biavati, G., Bidlot, J., Bonavita, M., De Chiara, G., Dahlgren, P., Dee, D., Diamantakis, M., Dragani, R., Flemming, J., Forbes, R., Fuentes, M., Geer, A., Haimberger, L., Healy, S., Hogan, R. J., Hólm, E., Janisková, M., Keeley, S., Laloyaux, P., Lopez, P., Lupu, C., Radnoti, G., de Rosnay, P., Rozum, I., Vamborg, F., Villaume, S., and Thépaut, J. N.: The ERA5 global reanalysis, Q. J. R. Meteorol. Soc., 146, 1999–2049, https://doi.org/10.1002/qj.3803, 2020.

Immerzeel, W. W., Van Beek, L. P. H., and Bierkens, M. F. P.: Climate change will affect the asian water towers, Science (80-.)., 328, 1382–1385, https://doi.org/doi: 10.1126/science.1183188, 2010.

Khadka, A.: NGS Mount Everest AWS Network, (Version 2), Zenodo [data set], https://doi.org/10.5281/zenodo.18849098, 2026.

Khadka, A., Matthews, T., Perry, L. B., Koch, I., Wagnon, P., Shrestha, D., Sherpa, T. C. G., Aryal, D., Tait, A., Sherpa, T. C. G., Tuladhar, S., Baidya, S. K., Elvin, S., Elmore, A. C., Gajurel, A., and

https://doi.org/10.5194/essd-2026-183
Preprint. Discussion started: 23 April 2026

Mayewski, P. A.: Weather on Mount Everest during the 2019 summer monsoon, Weather, 76, 205–207, https://doi.org/10.1002/wea.3931, 2021.

Khadka, A., Wagnon, P., Brun, F., Shrestha, D., Lejeune, Y., and Arnaud, Y.: Evaluation of ERA5-Land and HARv2 reanalysis data at high elevation in the upper Dudh Koshi basin (Everest region, Nepal), J. Appl. Meteorol. Climatol., 61, 931–954, https://doi.org/10.1175/jamc-d-21-0091.1, 2022.

King, O., Bhattacharya, A., Ghuffar, S., Tait, A., Guilford, S., Elmore, A. C., and Bolch, T.: Six Decades of Glacier Mass Changes around Mt. Everest Are Revealed by Historical and Contemporary Images, One Earth, 3, 608–620, https://doi.org/10.1016/J.ONEEAR.2020.10.019, 2020.

Kochendorfer, J., Earle, M., Rasmussen, R., Smith, C., Yang, D., Morin, S., Mekis, E., Buisan, S., Roulet, Y.-A., Landolt, S., Wolff, M., Hoover, J., Thériault, J. M., Lee, G., Baker, B., Nitu, R., Lanza, L., Colli, M., Meyers, T., Kochendorfer, J., Earle, M., Rasmussen, R., Smith, C., Yang, D., Morin, S., Mekis, E., Buisan, S., Roulet, Y.-A., Landolt, S., Wolff, M., Hoover, J., Thériault, J. M., Lee, G., Baker, B., Nitu, R., Lanza, L., Colli, M., and Meyers, T.: How Well Are We Measuring Snow Post-SPICE?, Bull. Am. Meteorol. Soc., 103, E370–E388, https://doi.org/10.1175/BAMS-D-20-0228.1, 2022.

Matthews, T., Perry, L. B., Koch, I., Aryal, D., Khadka, A., Shrestha, D., Abernathy, K., Elmore, A. C., Seimon, A., Tait, A., Elvin, S., Tuladhar, S., Baidya, S. K., Potocki, M., Birkel, S. D., Kang, S., Sherpa, T. C., Gajurel, A., and Mayewski, P. A.: Going to Extremes: Installing the World's Highest Weather Stations on Mount Everest, Bull. Am. Meteorol. Soc., 101, E1870–E1890, https://doi.org/10.1175/BAMS-D-19-0198.1, 2020a.

Matthews, T., Perry, L. B., Lane, T. P., Elmore, A. C., Khadka, A., Aryal, D., Shrestha, D., Tuladhar, S., Baidya, S. K., Gajurel, A., Potocki, M., and Mayewski, P. A.: Into Thick(er) Air? Oxygen Availability at Humans' Physiological Frontier on Mount Everest, iScience, 23, 101718, https://doi.org/10.1016/j.isci.2020.101718, 2020b.

Matthews, T., Perry, B., Khadka, A., Sherpa, T. G., Shrestha, D., Aryal, D., Tuldahar, S., Thapa, N., Pradhananga, N., Athans, P., Sherpa, D. Y., Guy, H., Seimon, A., Elmore, A., Li, K., and Alexiev, N.: Weather observations reach the summit of Mount Everest, Bull. Am. Meteorol. Soc., 1, https://doi.org/10.1175/BAMS-D-22-0120.1, 2022.

Miner, K. R., Mayewski, P. A., Baidya, S. K., Broad, K., Clifford, H., Elmore, A., Gajurel, A. P., Giri, B., Guilford, S., Hubbard, M., Jaskolski, C., Koldewey, H., Li, W., Matthews, T., Napper, I., Perry, L. B., Potocki, M., Priscu, J. C., Tait, A., Thompson, R., and Tuladhar, S.: An overview of physical risks in the Mt. Everest region, cell.com, 3, 547–550, https://doi.org/10.1016/j.oneear.2020.10.008, 2020.

Perry, L. B., Matthews, T., Guy, H., Koch, I., Khadka, A., Elmore, A. C., Shrestha, D., Tuladhar, S., Baidya, S. K., Maharjan, S., Wagnon, P., Aryal, D., Seimon, A., Gajurel, A., and Mayewski, P. A.: Precipitation Characteristics and Moisture Source Regions on Mt. Everest in the Khumbu, Nepal, One Earth, 3, 594–607, https://doi.org/10.1016/j.oneear.2020.10.011, 2020.

Pfeffer, W. T., Arendt, A. A., Bliss, A., Bolch, T., Graham, J., Gardner, A. S., Hagen, J.-O., Hock, R., Kaser, G., Kienholz, C., Miles, E. S., Moholdt, G., Mo¨lg, N., Mo¨lg, M., Paul, F., Radic´, V., Radic´, R., Rastner, P., Raup, B. H., Rich, J., Sharp, M. J., and Consortium, R.: The Randolph Glacier Inventory: a globally complete inventory of glaciers, https://doi.org/10.3189/2014JoG13J176, 2014.

Potocki, M., Mayewski, P. A., Matthews, T., Perry, L. B., Schwikowski, M., Tait, A. M., Korotkikh, E., Clifford, H., Kang, S., Sherpa, T. C., Singh, P. K., Koch, I., and Birkel, S.: Mt. Everest's highest glacier is

https://doi.org/10.5194/essd-2026-183
Preprint. Discussion started: 23 April 2026

417 a sentinel for accelerating ice loss, npj Clim. Atmos. Sci., 5, 1–8, https://doi.org/10.1038/s41612-022-
418 00230-0, 2022.

419 Salerno, F., Guyennon, N., Thakuri, S., Viviano, G., Romano, E., Vuillermoz, E., Cristofanelli, P.,
420 Stocchi, P., Agrillo, G., Ma, Y., and Tartari, G.: Weak precipitation, warm winters and springs impact
421 glaciers of south slopes of Mt. Everest (central Himalaya) in the last 2 decades (1994-2013), Cryosph., 9,
422 1229–1247, https://doi.org/10.5194/tc-9-1229-2015, 2015.

423 Salerno, F., Guyennon, N., Yang, K., Shaw, T. E., Lin, C., Colombo, N., Romano, E., Gruber, S., Bolch,
424 T., Alessandri, A., Cristofanelli, P., Putero, D., Diolaiuti, G., Tartari, G., Verza, G., Thakuri, S., Balsamo,
425 G., Miles, E. S., and Pellicciotti, F.: Local cooling and drying induced by Himalayan glaciers under global
426 warming, Nat. Geosci., 16, 1120–1127, https://doi.org/10.1038/s41561-023-01331-y, 2023.

427 Shea, J. M., Wagnon, P., Immerzeel, W. W., Biron, R., Brun, F., and Pellicciotti, F.: A comparative high-
428 altitude meteorological analysis from three catchments in the Nepalese Himalaya, Int. J. Water Resour.
429 Dev., 31, 174–200, https://doi.org/10.1080/07900627.2015.1020417, 2015.

430 Sherpa, T. C., Matthews, T., Perry, L. B., Thapa, A., Singh, P. K., Khadka, A., Koch, I., Pelto, M.,
431 Panday, P., Aryal, D., Shrestha, D., Kang, S., and Mayewski, P. A.: Insights from the first winter weather
432 observations near Mount Everest's summit, Weather, 1–5, https://doi.org/10.1002/wea.4374, 2023.

433 Thakuri, S., Salerno, F., Smiraglia, C., Bolch, T., D'Agata, C., Viviano, G., and Tartari, G.: Tracing
434 glacier changes since the 1960s on the south slope of Mt. Everest (central Southern Himalaya) using
435 optical satellite imagery, Cryosph., 8, 1297–1315, https://doi.org/10.5194/tc-8-1297-2014, 2014.

436 Thakuri, S., Dahal, S., Shrestha, D., Guyennon, N., Ramano, E., and Colombo, N.: Elevation-dependent
437 warming of maximum air temperature in Nepal during 1976–2015, Atmos. Res., 228, 261–269,
438 https://doi.org/https://doi.org/10.1016/j.atmosres.2019.06.006, 2019.

439 THT: NatGeo scientists instal highest weather station on Mt Everest - The Himalayan Times, 2022.

440 Wagnon, P., Brun, F., Khadka, A., Berthier, E., Shrestha, D., Vincent, C., Arnaud, Y., Six, D., Dehecq,
441 A., Ménégoz, M., and Jomelli, V.: Reanalysing the 2007-19 glaciological mass-balance series of Mera
442 Glacier, Nepal, Central Himalaya, using geodetic mass balance, J. Glaciol., 67, 117–125,
443 https://doi.org/10.1017/jog.2020.88, 2021.

444 Van Wyk de Vries, M., Matthews, T., Perry, L. B., Thapa, N., and Wilby, R.: At-scale Model Output
445 Statistics in mountain environments (AtsMOS v1.0), Geosci. Model Dev., 17, 7629–7643,
446 https://doi.org/10.5194/gmd-17-7629-2024, 2024.

447 Yang, W., Guo, X., Yao, T., Yang, K., Zhao, L., Li, S., Zhu, M., Yang, W., Guo, X., Yao, T., Yang, K.,
448 Zhao, L., Li, S., and Zhu, M.: Summertime surface energy budget and ablation modeling in the ablation
449 zone of a maritime Tibetan glacier, J. Geophys. Res. Atmos., 116, 14116,
450 https://doi.org/10.1029/2010JD015183, 2011.

451

452